Monitoring the generation and propagation of ionospheric disturbances and effects on Global Navigation Satellite System positioning

S. M. Stankov,[1] N. Jakowski,[1] K. Tsybulya,[1] and V. Wilken[1]

Received 8 August 2005; revised 10 March 2006; accepted 8 May 2006; published 12 August 2006.

[1] To gain a more comprehensive view of the powerful and dynamic plasma processes occurring during ionospheric storms, ground- and space-based observations using Global Navigation Satellite System (GNSS) signals have been analyzed. Several case and statistical studies of ionospheric storms are presented, clearly showing the generation and propagation of ionospheric disturbances. Discussed are the capabilities of advanced techniques for routine monitoring of the ionosphere and studying the ionospheric perturbations. It is concluded that the permanent monitoring of the ionosphere-plasmasphere system can play a significant role in mitigating adverse space weather effects on GNSS-based positioning.

Citation: Stankov, S. M., N. Jakowski, K. Tsybulya, and V. Wilken (2006), Monitoring the generation and propagation of ionospheric disturbances and effects on Global Navigation Satellite System positioning, *Radio Sci.*, *41*, RS6S09, doi:10.1029/2005RS003327.

1. Introduction

[2] Ionospheric storms, being extreme forms of space weather, can adversely affect the performance of present-day communication and navigation systems. In relation to this, there are currently some major challenges facing the ionospheric specialists: the development of geomagnetic storms and the impact that storms have on ionospheric behavior, development and evolution of ionospheric inhomogeneities/irregularities, development of methods for ionospheric predictions, etc. [*Goodman*, 2005]. Therefore it is important to understand the mechanisms behind the ionospheric perturbations, to know their spatial development and propagation patterns, to identify the whole spectrum of possible adverse effects, to monitor the space weather and ionosphere characteristics, and ultimately to try to predict the effects of those perturbations.

[3] Over the years, theoretical and empirical research improved significantly our understanding of the ionospheric storms and associated disturbances. Thus it is now clear that the ionospheric storms go through an initial "positive" phase, when the electron density and the electron content are greater than the normal median values, followed by the main "negative" phase when the above quantities are reduced below their normal pre-event values [*Proelss*, 1995]. Several mechanisms have been proposed to explain the positive phase: thermospheric winds reducing the ion loss and increasing the ion production during daytime, plasma uplifting due to thermospheric winds or electric fields, neutral gas downwelling that decreases the recombination rate, etc. The negative phase is commonly explained with the increased N_2/O density ratio that leads to increased ion loss rate resulting in decreased plasma density. During storms, large variations in the main ionospheric parameters are observed. In general, the ionospheric perturbations propagate in the equatorward direction, the speed and extent of this penetration depending strongly on local time and season. The velocity is estimated to be on the order of 400–900 m s^{-1}, and theoretically, because of the reduced ion drag during night, the propagation should be much faster and more extensive in the nighttime rather than in the daytime hemisphere [*Foerster and Jakowski*, 2000].

[4] The principle behind the differential Global Navigation Satellite System (GNSS)-based precise positioning is for a reference receiver to be located at a base station with known coordinates, while another receiver's coordinates are determined relative to the reference receiver. Real-time GNSS precise positioning is one of the most progressive technological innovations, even making it possible for the GNSS receiver to be in motion. Such systems are referred to as real-time kine-

[1]German Aerospace Center, Institute of Communications and Navigation, Neustrelitz, Germany.

0048-6604/06/2005RS003327

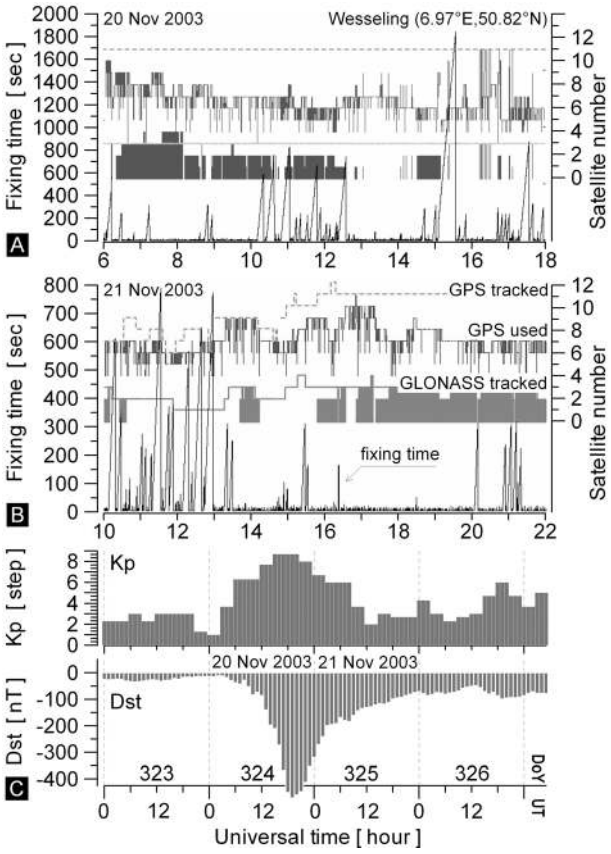

Figure 1. Ambiguity fixing time, as monitored on (a) 20 November 2003 and (b) 21 November 2003. (c) The severe geomagnetic storm started on 20 November, with *Kp* reaching 8.67 and *Dst* values dropping far below the −400 mark in the evening hours. Frequent occurrences of increased ambiguity fixing time (occasionally exceeding 10 min) have been observed during both the main and the recovery phase of the storm. Notice the decreased number of tracked and used GPS satellites.

matic (RTK) systems and are widely used in engineering and navigation applications. However, the use of GNSS carrier phase data comes at a cost because the measurements are ambiguous and require the utilization of ambiguity resolution, cycle slip removal, and other processing algorithms [*Blewitt*, 1990]. Therefore a very important factor determining the performance of the GNSS reference network services is the time required to solve the phase ambiguities supposedly affected, among other factors, by the ionospheric disturbances [*Wanninger*, 2004]. A case is presented here (Figure 1) when frequent occurrence of relatively long fixing times (exceeding 600 s) was observed during the disturbed days of 20 and 21 November 2003. Cases of longer fixing times during storms and even extreme cases of failures in resolving the ambiguities have been reported [*Jakowski et al.*, 2005]. Prolonged and/or frequent increases of the fixing times may have adverse impact on GNSS positioning and safety-critical applications. Another important parameter to watch is the number of tracked/used GNSS satellites for each ground receiving station. It is essential to track as many GNSS satellites as possible because some of them cannot be used because of restrictions imposed on the satellite elevation angle (elevation cutoff criterion), signal-to-noise ratio (SNR) criterion, etc. Data from the remaining satellites can be processed and used for fixing the ambiguities. Since further restrictions are imposed on the solution, including limitations on error magnitude and requirements for stability of solution, the number of the "processed" satellites should not be less than five to ensure that the reference services are reliable [*Trimble Navigation, Ltd.*, 2005]. Now, as it is obvious that the strong ionospheric perturbations do affect the determination of phase ambiguities, and considering the fact that the ionosphere contributes to the largest error in RTK services in terms of reliability and availability, it is important to find ways to mitigate all ionosphere-induced problems in GNSS-based applications [*Chen et al.*, 2003]. A crucial step in the mitigation process is the prediction of the ionospheric behavior [*Jakowski et al.*, 2002b; *Stankov et al.*, 2004].

[5] While theories explaining most aspects of the ionospheric behavior exist in abundance and are generally accepted, the theories themselves do not always deliver sufficiently good prediction of the ionospheric behavior. The models—theoretical, empirical, or semi-empirical—are not always helpful because the driving forces and/or boundary conditions are not always known or available [*Stankov*, 1996], and therefore all models need reliable "update" schemes to be developed, implemented, and maintained. The situation is even more difficult when trying to predict the ionospheric effects on the performance of communication and navigation systems. All these considerations underline the importance, actually the inevitable necessity of permanently monitoring the ionospheric state. It should be stressed that such monitoring should be complex, involving simultaneous ground- and space-based observations [*Jakowski*, 1996; *Jodogne and Stankov*, 2002; *Stankov et al.*, 2003b].

[6] In order to obtain/provide more insight into the ionosphere-plasmasphere behavior under both quiet and storm time conditions, the German Aerospace Center (DLR) developed a total electron content (TEC) monitoring service over the European and polar regions [*Jakowski*, 1996]. Apart from measuring the total ionization, the service also helped research the slab thickness behavior at several ionosonde locations in Europe. In addition, ionospheric radio occultation (IRO) measure-

ments [*Jakowski et al.*, 2002a] have been used to study the global ionospheric behavior, particularly the small- and medium-scale irregularities that are known to cause problems in GNSS-based applications. Furthermore, the DLR established a specific ionosphere/space weather monitoring system [*Jakowski et al.*, 2005]. This novel operational system collects various types of information on the past, actual, and predicted state of the ionosphere and plasmasphere; processes the data immediately; and delivers real-time data products, such as TEC maps, TEC spatial and temporal gradient maps, cycle slip number, geophysical condition warnings, etc. The service is offered to scientific and industry users and educational and general public structures. Finally, assessed is the feasibility of implementing a new index that is more closely related to the ionospheric effects and that is oriented toward the user needs for high-precision GNSS positioning.

2. Ground-Based GNSS Observations

[7] Space weather–induced disturbances in the ionosphere are characterized by large variations in the vertical and horizontal electron density distribution. Ground-based GNSS measurements can be used for estimating the horizontal distribution of TEC on regional and global scales. DLR has been operating a system for regularly processing ground-based Global Positioning System (GPS) data and producing maps of the integrated electron content over the European and polar regions since 1995 [*Jakowski*, 1996]. The GPS data, obtained mainly from the International GNSS Service (IGS) stations [*Beutler et al.*, 1999], allow the determination of slant TEC values along numerous satellite-receiver links. After calibration, the slant TEC data are mapped to the vertical axis by utilizing a mapping function based on a single ionospheric layer approximation set at h = 400 km. Afterward, the measurements are assimilated into a regional TEC model [*Jakowski et al.*, 1998] in which the TEC value is expressed by

$$TEC = \sum_{i=0}^{2}\sum_{j=0}^{2}\sum_{k=0}^{1}\sum_{n=0}^{1} T_i(t)S_j(d)A_k(F_{10.7})L_n(\varphi_m), \quad (1)$$

where the term T represents the diurnal variation, S the seasonal variation, A the solar activity dependence, and L the dependence on geomagnetic latitude. The formula coefficients are computed by least squares fitting to the measurements. These coefficients are regularly updated in line with the changing solar activity. In general, the modeling procedure ensures that the final TEC map provides the real measurement values at the observation points and model values over areas without observations. For the polar maps, the vertical TEC values are computed on a grid consisting of 768 points; the grid covers the geographic latitude range from 50°N to 90°N, spacing 2.5°, and the geographic longitude range from 0°E to 360°E, spacing 7.5°. Thus it is possible to image and monitor large-scale perturbations in the entire polar/auroral zone.

[8] Enhanced space weather impact is expected first on the high-latitude ionosphere because of the much stronger coupling with the magnetosphere and the solar wind. The high-latitude electric field, the precipitation of energetic particles, and the plasma convection are reportedly the most powerful driving forces for the highly dynamic and complex processes taking place in this region [*Jakowski et al.*, 1992]. During geomagnetic storms, the enhancements in the solar wind energy cause large perturbations in the high-latitude ionosphere and thermosphere, resulting in significant variability of the plasma density which propagates toward lower latitudes. Therefore regular monitoring of the total ionization at high latitudes can significantly improve our understanding of the complex coupling processes between the solar wind, magnetosphere, ionosphere, and thermosphere and, ultimately, on the generation of ionospheric disturbances.

[9] The propagating plasma patches are some of the less studied types of ionospheric irregularities [*Tsunoda*, 1988]. The plasma patches are regions of enhanced plasma density, several times higher than the background density. The patches appear in the cusp region, usually when the interplanetary magnetic field (IMF) is directed southward, and drift across the polar cap driven by the magnetospheric convection. Some theories explain the patch formation with plasma convection instabilities in a tongue of ionization formed by plasma convection transporting plasma from dayside to nightside regions. Patches may also arise after particle precipitation events in the polar cap. For example, on the background of already increased TEC, a patch of higher ionization was detected in the plots of the polar region during the onset of the storm beginning 7 November 2004 (Figure 2). The patch appeared near the geographic pole at about 1300 UT and grew in size while also moving southward. Strong increase in the ionization, accompanied by particle precipitation and plasma convection patterns, typical for the ionospheric storm onset, developed at 1700 UT.

[10] A very useful quantity for investigating the propagation of ionospheric disturbances is the relative deviation, ΔTEC, of the observed TEC value from its (monthly) median, TEC_{med}, that is, $\Delta TEC = (TEC - TEC_{\mathrm{med}})/TEC_{\mathrm{med}}$. The analysis and interpretation of the perturbation effects is far easier when this ratio is used rather than the absolute TEC value. Presented next are results from two recent storms, in July and November 2004.

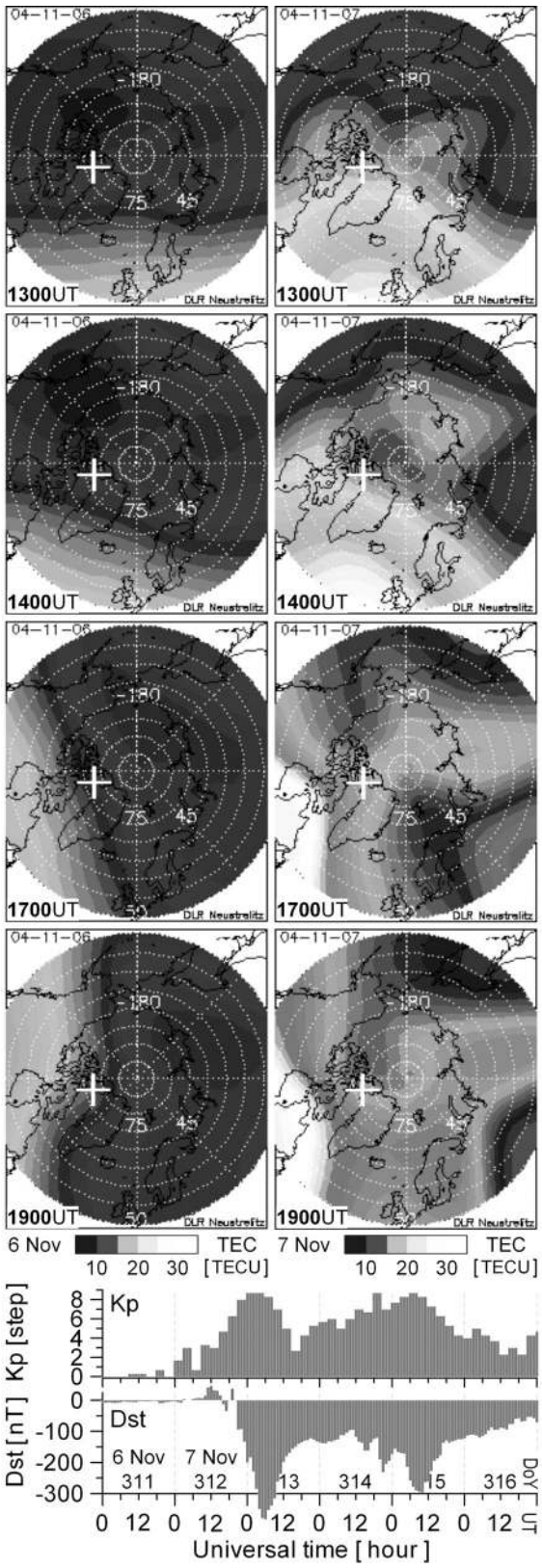

[11] The last days of July 2004 were remarkably active considering the approaching solar minimum of the current cycle. Three major storm events occurred, with *Dst* index reaching −104 nT on 23 July, −150 nT on 25 July, and −167 nT on 27 July. The IMF and geomagnetic fields were seriously disturbed, and several problems were reported by GNSS users. The observed increase of relative TEC between 0600 and 1400 UT (Figure 3, left plots) indicates the action of an eastward directed electric field which penetrates from high latitudes toward lower latitudes and lifts up the plasma by $\mathbf{E} \times \mathbf{B}$ drift, resulting in a reduced loss rate, that is, in a positive ΔTEC response. As a natural consequence of the high-latitude heating and expansion, equatorward directed neutral winds are generated that lift up the plasma along geomagnetic field lines. Since this process is most effective near 65° geomagnetic inclination, the observed peak of ionization at 45°N supports this interpretation quite well. Furthermore, a neutral wind–induced plasma uplifting process is characterized by a delayed response at lower latitudes [*Foerster and Jakowski*, 2000].

[12] Indications of an upcoming storm are clearly seen on the polar maps as early as 1300 UT on 7 November 2004 (Figure 2, top right). As the European ΔTEC maps show (Figure 3, right plots), an area of higher ionization appeared in the north at 1600 UT which expanded and propagated toward lower latitudes and notably increased the TEC over the entire continent. However, the ionization peak did not propagate below 50°N latitude. This behavior obviously differs from the above-described storm time behavior in summer and is due to the occurrence of some resistance forces at these latitudes. Such seasonal difference can be explained by thermospheric winds blowing preferentially from the summer to the winter hemisphere and so being in phase (during summer) or antiphase (during winter) with the perturbation-induced winds directed equatorward. While it is true that the ionospheric variability is fueled by the energy coming from the Sun, it is clear that secondary energy sources from below the ionosphere may also be significant. Therefore the role played by the thermospheric winds cannot be neglected; they are actually capable of forcing the ionospheric response for particular conditions. For example, distinct ionospheric responses are observed for winter conditions at 20°–40° and at

Figure 2. Ground-based GPS TEC observation of the North Pole region for the ionospheric storm events that started on 7 November 2004. For comparison, the corresponding maps from the previous, quiet day are also provided. The geomagnetic pole is marked with a cross on each plot.

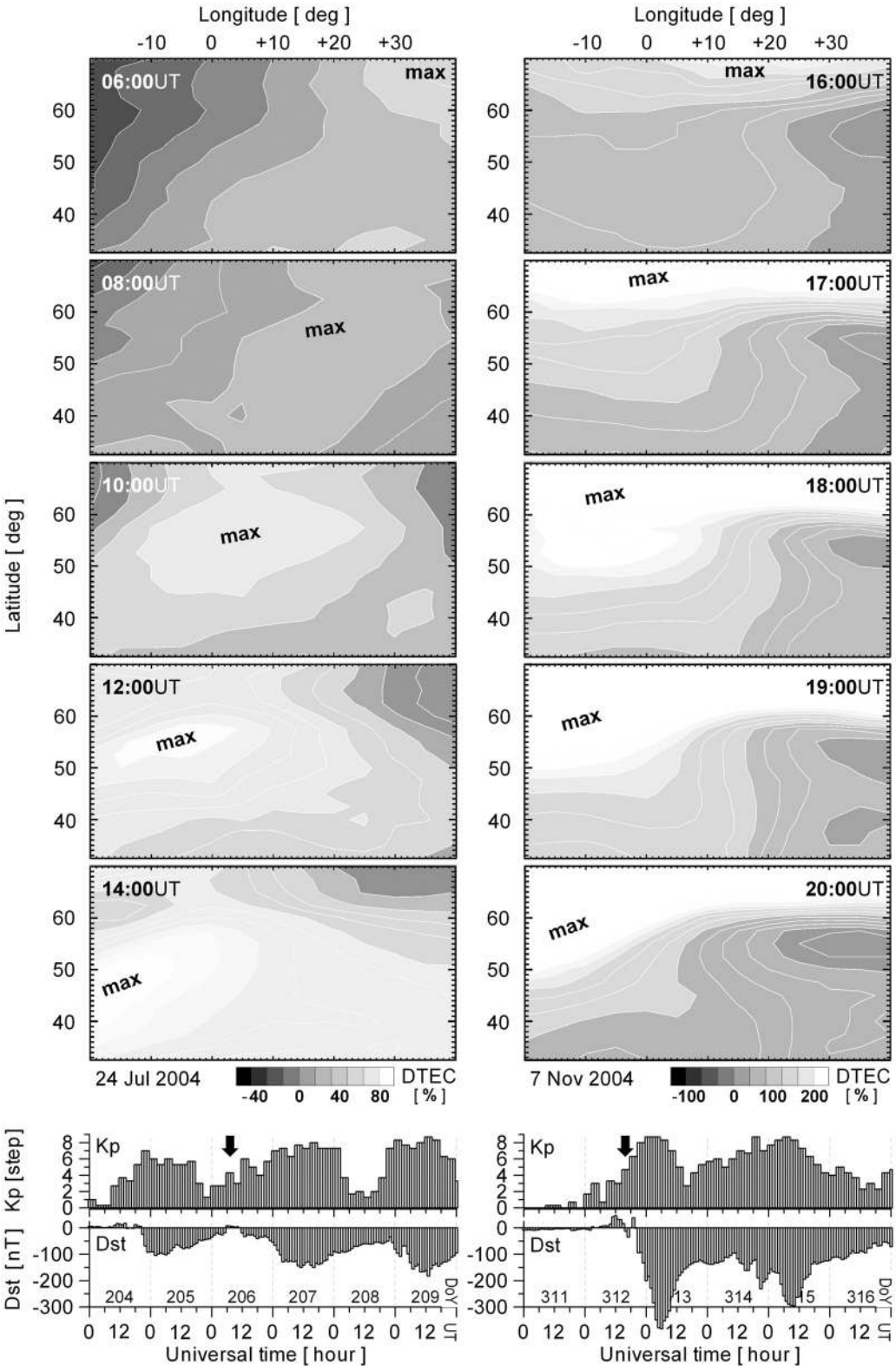

Figure 3. Relative TEC on (left) 24 July 2004 and (right) 7 November 2004.

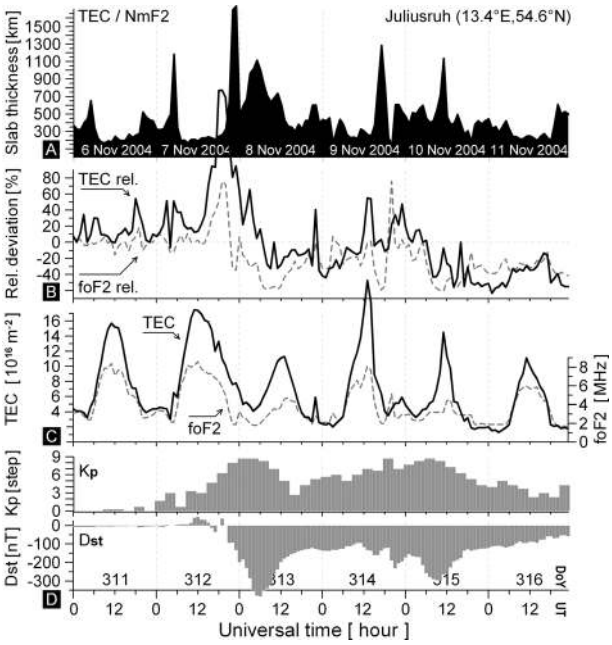

Figure 4. (a) Operational monitoring of the slab thickness (TEC/N_mF_2) for the site of Juliusruh (13.4°E, 54.6°N) during the period of 6–11 November 2004. (b) Relative deviations from medians, TEC_{rel} = (TEC − TEC_{med})/TEC_{med} and f_oF_{2rel} = (f_oF_2 − f_oF_{2med})/f_oF_{2med}, (c) corresponding TEC and f_oF_2 measurements, and (d) *Kp* and *Dst* indices are also plotted. The median values are calculated over the period from 23 October to 18 November 2004. The slab thickness calculations are presented "as is" in order to demonstrate operational capabilities. Data gaps do occur from time to time, predominantly in f_oF_2, but it is possible to implement efficient procedures for temporal interpolation [*Muhtarov and Kutiev*, 1999].

40°–60° geomagnetic latitudes [*Araujo-Pradere and Fuller-Rowell*, 2002; *Araujo-Pradere et al.*, 2004].

[13] DLR established an operational system that monitors the TEC over Europe and the ionospheric slab thickness (τ = TEC/N_mF_2) at sites of the European digital ionosondes. The slab thickness contains information on the neutral/plasma temperatures and delivers crucial information on both the topside and bottomside ionospheric behavior during geomagnetic storms. Wide variability of this parameter during storms is reported, suggesting that significant vertical redistributions of plasma take place in such periods. As an example, results are presented from the ionospheric storm that started on 7 November 2004 (Figure 4). The positive phase, beginning in the early afternoon, is well seen in both the f_oF_2 and TEC measurement plots when the percentage deviations from medians surges about 80% for f_oF_2 and more than 150% for TEC. As a result, only a slight increase is observed in the slab thickness values in the afternoon. However, the thickness rose sharply in the evening because of decreasing f_oF_2 values and a longer-lasting TEC positive phase. In theory, increased TEC, accompanied by constant or decreasing f_oF_2 (i.e., growing slab thickness) indicates a process of plasma uplifting. In such cases, the perturbation of the vertical electron density structure is localized in the topside ionosphere. High slab thickness values during nighttime may indicate the occurrence of enhanced plasma fluxes from the plasmasphere, for example, because of compression of the geomagnetic field during the onset phase of the storm [*Jakowski*, 1981; *Jakowski and Lois*, 1984]. The date 8 November is characterized by a seriously perturbed and depleted ionosphere, resulting in lower than average f_oF_2 and TEC values. However, TEC surged again on 9 and 10 November, exceeding 22 TECU (1 TECU = 10^{16} el m^{-2}) and not matched by concurrent f_oF_2 increase, resulting in strong enhancements in the slab thickness. Probably more interesting is the slab thickness increase observed in the early morning hours of 7 November before the nominal start of the storm. Although the predawn increase in τ is a well-known feature, and the day-to-day variability is also known to be large, it is still difficult to explain this twofold increase compared with previous quiet time increases. The occurrences of slab thickness spikes correlate well with the peaks in *Kp* and *Dst* indices. It is clear that slab thickness measurements, if available in real time and for several suitable locations (for example, at several latitudes along a meridian), can be successfully used for monitoring and eventually predicting the propagation of ionospheric disturbances.

3. Space-Based GNSS Observations

[14] The ionospheric radio occultation (IRO) measurements onboard low Earth orbit (LEO) satellites can be utilized for global monitoring of the ionospheric and plasmaspheric ionization and for detecting ionospheric disturbances and irregularities. In this study, IRO measurements from the Challenging Minisatellite Payload (CHAMP) satellite (inclination 87°, altitude 450 km, launched 15 July 2000) have been used. Low-rate, 0.1 Hz sampled navigation data obtained with the zenith viewing antenna are used for reconstructing the topside ionosphere electron density distribution by data assimilation [*Heise et al.*, 2002]. Another method involving oversatellite TEC and ground f_oF_2 measurements is applied for reconstruction of the electron density from the bottom of the ionosphere up to the GPS height [*Stankov et al.*, 2003a; *Stankov et al.*, 2005]. Medium-rate, 1 Hz sampled occultation data from the limb-

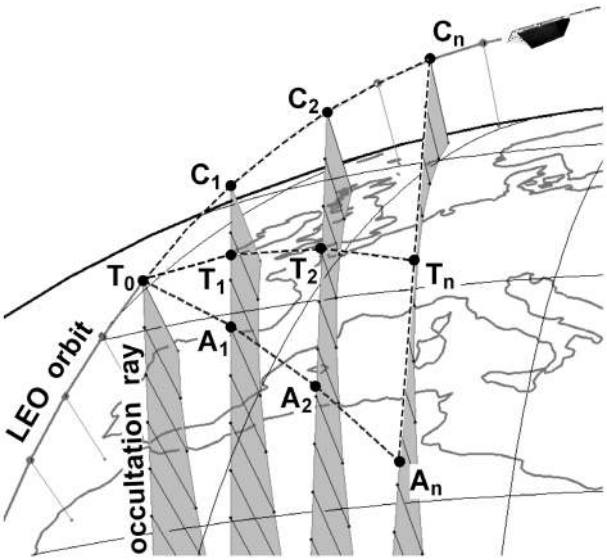

Figure 5. Geometry of an occultation event.

viewing antenna can be used for electron density profiling below the CHAMP orbit height. The dual-frequency carrier phases of the GPS signals are used to compute the total electron content along the occultation ray paths. Electron density profiles are then obtained with the help of a tomographic algorithm [*Jakowski et al.*, 2002a]. The reconstructed electron profiles allow the global observation of the topside ionospheric scale height even during geomagnetic storms [*Stankov and Jakowski*, 2006].

[15] An occultation event (Figure 5) is defined by the series of TEC measurements performed along the GPS-LEO occultation ray paths starting from the initial moment when a GPS satellite becomes "visible" from the receiver (at point T_0) until the moment this GPS satellite is obscured by the Earth (at point C_n). While CHAMP moves along its polar orbit, the occultation ray gets closer and closer to the Earth's surface, thus scanning the ionosphere from top to bottom. The occultation area A_j covered during the occultation event j is defined as the curvilinear triangle $\Delta T_0 C_n A_n$, where C_i is the CHAMP trajectory point, T_i is the tangent point (the closest point to the Earth's surface) on the ith occultation ray, and $A_i T_i = C_i T_i$, $i = 1,2,\ldots,n$. Thus the time of the occultation event is the middle of the occultation period and the geographic location is the location of the tangent point at the middle of the event.

[16] Profiles of the differential TEC, together with the corresponding vertical profiles of electron density, can be used directly for analysis of ionospheric storm effects (Figure 6). During the first occultation (Figure 6, top), performed just before the start of the July 2004 storm, a "regular," rather smooth profile was obtained. Depleted profiles were observed later during the storm, clearly demonstrating the storm's negative phase (Figure 6, middle). In addition, both the TEC and electron profiles were not smooth anymore and had irregular features. An extreme case is also presented (Figure 6, bottom) to demonstrate how severe the ionosphere disturbances can be. These examples lead to the question of how the irregularities can be monitored and quantified via IRO observations.

[17] Apart from the regularly occurring large-scale ionospheric gradients/processes (due to solar activity, local time, season, etc.), medium- and small-scale irregularities, occurring in certain areas and periods, may also affect radio wave propagation and communications [*Rawer*, 1993]. A major objective achieved with the IRO observations is the detection and investigation of ionospheric irregularities with characteristic size ranging from a few kilometers to several hundreds of kilometers. Larger-scale structures cannot be observed because the ionospheric region covered by an occultation event is rather limited. Smaller structures and high-frequency oscillations cannot be detected because the GPS

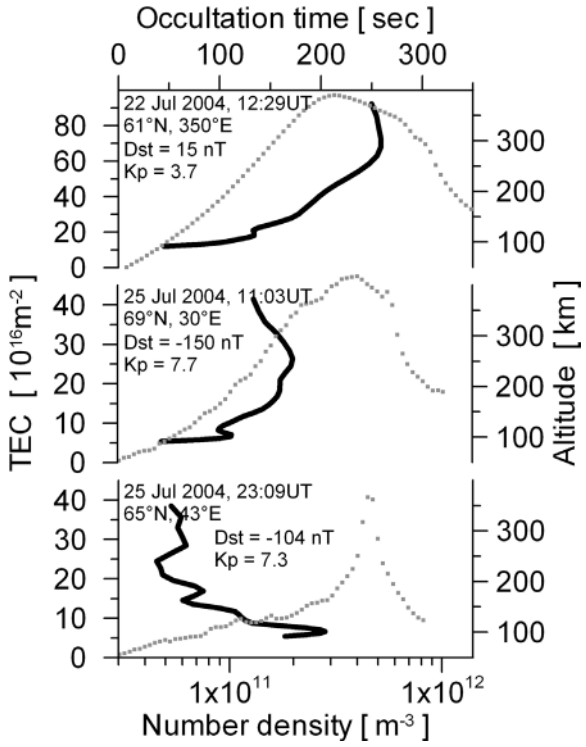

Figure 6. IRO measurement samples of (left versus top axis) the differential TEC (dotted lines) along the occultation ray path used for (right versus bottom axis) electron density profiles (solid lines) inversion before and during the July 2004 storm.

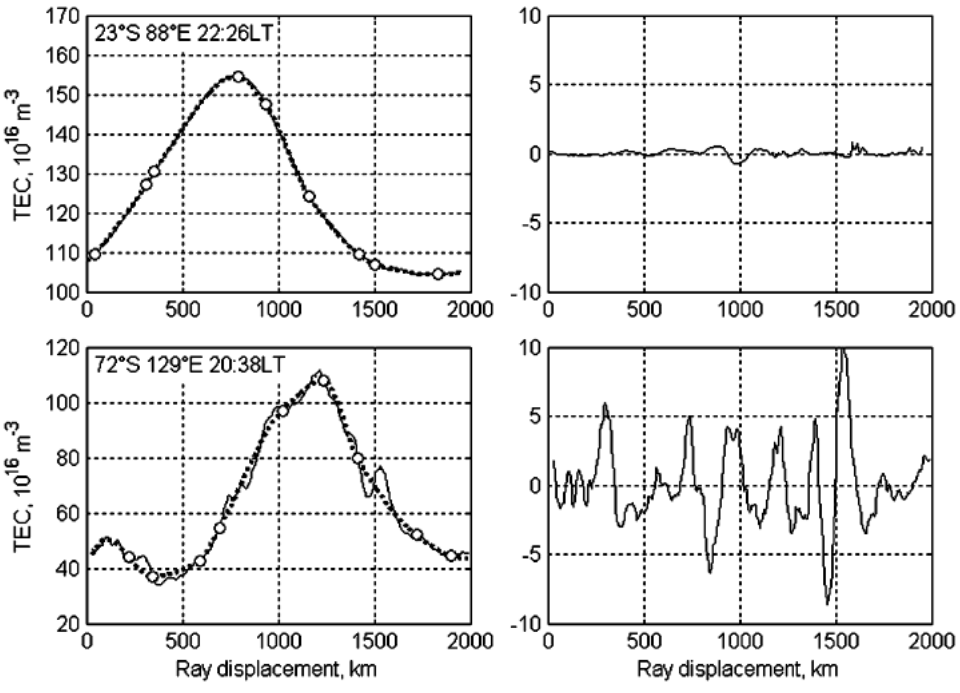

Figure 7. Ionospheric irregularities deduced from CHAMP IRO measurements: (top left) typical occultation TEC profile with regular smooth features, in contrast to (bottom left) another TEC profile having features that clearly indicate the presence of ionospheric irregularities. The differences between the measured TEC profiles and their corresponding nine-point cubic approximations are plotted on the right side.

receivers have a limited data sampling rate. Therefore the focus is on the ionospheric F region irregularities only. Since the irregularities affect the TEC profile shape (Figure 7), we can use a mathematical quantity that can provide a reliable estimate of the TEC profile smoothness (actually, the profile roughness). For this purpose, first the occultation measured $TEC(s)$ is approximated by a polynomial $P(s)$, and then the difference between the measured and approximated TEC is calculated, $TEC_{\mathrm{pol}}(s) = TEC(s) - P(s)$. This difference is further divided by the maximal value of $TEC(s)$ in order to obtain the TEC gradient, $TEC'(s)$. Actually, $TEC'(s)$ shows how intensive the variations of TEC are because of the ionospheric irregularities. Finally, the root-mean-square (RMS) of the gradient (in units of TECU km^{-1}) is calculated:

$$G_{\mathrm{RMS}} = \sqrt{\frac{1}{D}\int_0^D \left(\frac{d}{ds}TEC(s)\right)^2 ds}, \qquad (2)$$

where s is the occultation ray displacement, that is, the distance passed by the occultation tangent point. During each occultation event, the parameter s changes from 0 to the so-called "smear length," D (i.e., the maximal length of the tangent point's excursion during the occultation event, T_0T_n). Thus the RMS estimate serves as a generic measure of the ionospheric disturbance activity/intensity in the corresponding occultation area. In fact, a single RMS value, G^j_{RMS}, is assigned to the entire occultation area, A_j. During a certain time period, say from year 2002 to year 2005, a given geographical location happens to be within several occultation areas $\{A_j, j = 1,2,\ldots,m\}$ and thus is assigned several RMS values $\{G^j_{\mathrm{RMS}},\ j = 1,2,\ldots,m\}$. To create a map, the mean value $\overline{G^j_{\mathrm{RMS}}}$ is assigned to the given location.

[18] Although the above-described TEC gradient estimate is robust (i.e., not susceptible to polynomial approximation effects), the procedure itself does not allow clear separation of the irregularities of different scale. Therefore a better approach is to apply the Fourier transform to $TEC_{\mathrm{pol}}(s)$ and the average amplitude of the Fourier components within a given wavelength range to be calculated [*Press et al.*, 1992]. If a TEC profile has N data points, the nth spectral density is calculated by

$$S_n = \frac{D}{N-1}\sum_{j=1}^{N}\left\{TEC_j \exp[2\pi i(j-1)n - 1)/N]\right\}, \quad (3)$$

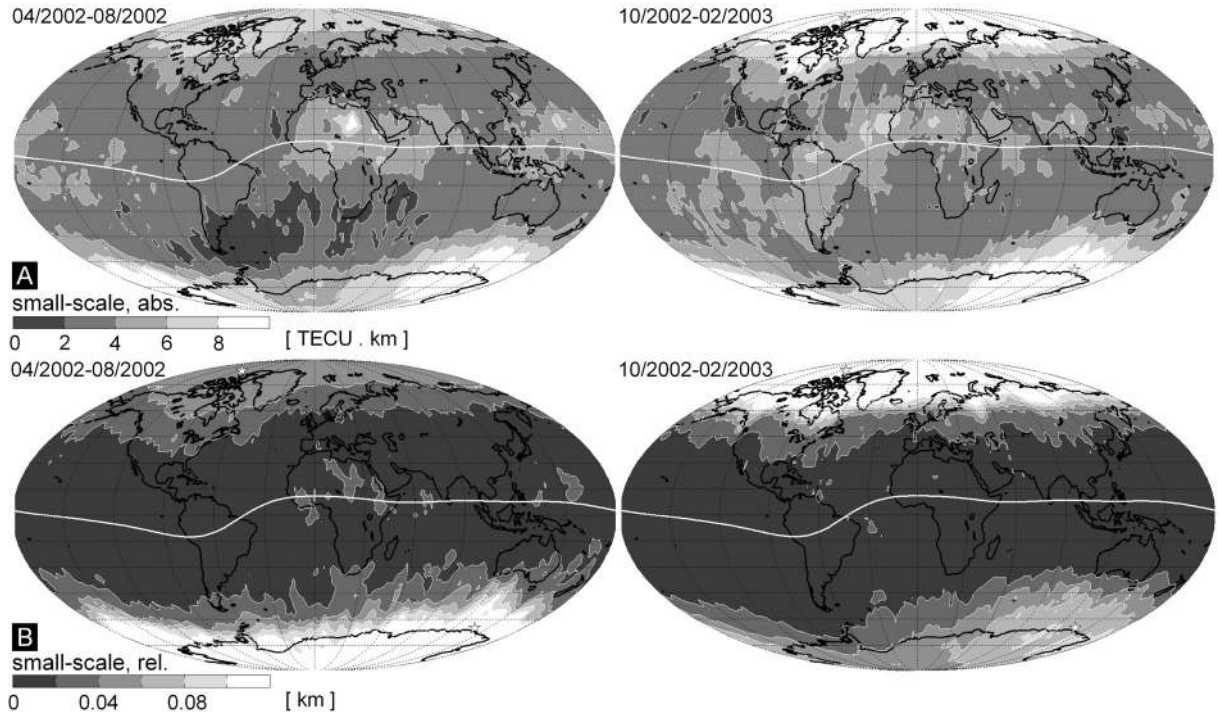

Figure 8. Small-scale ionospheric irregularities deduced from CHAMP IRO measurements: (a) absolute and (b) relative intensity of ionospheric irregularities obtained from CHAMP IRO measurements (left) from April to August 2002 and (right) from October 2002 to February 2003. The absolute values clearly show the increased intensity over the equatorial regions, while the relative values enhance the intensity of ionospheric irregularities over the polar areas; notice the particularly high intensity during winter.

where the term $D/(N - 1)$ is needed to convert the spectral density per data point to spectral density per unit of wave number. Also, the absolute value of S_n is used in order to discard the phase information contained in the original Fourier coefficient. Thus the averaged amplitudes for small-scale disturbances (wavelength 15–30 km) and medium-scale disturbances (80–150 km) can be used now as measures (at the corresponding scales) of the ionospheric inhomogeneities/disturbances in the occultation region. The spectral density algorithm has been applied to the CHAMP IRO measurements from March 2002 to February 2005, revealing small-scale (Figure 8) as well as medium-scale (Figure 9) ionospheric irregularities. The mapped value is the average spectral density, and since the spectral density is calculated per unit of inverse wavelength, the mapping is in units of TECU km^{-1}, and the grid resolution is 2° in geographic latitude and longitude. If the spectral density estimate (SDE) calculated for a TEC profile is divided by the maximal value of TEC in this profile, the effects that may be caused by differences in the electron density are removed. Thus the relative SDE mapping highlights several phenomena that are not visible on the absolute SDE maps. The maps show clearly the global distribution of ionospheric irregularities. It is obvious that in the polar regions, the irregularities have a high level of intensity. However, the occurrence frequency of ionospheric irregularities is higher in the periods of high magnetic and auroral activity. Such pronounced activity at higher latitudes in winter indicates the tracing of atmospheric gravity waves (AGW), actually small- and medium-scale traveling ionospheric disturbances (TID) coming from the auroral oval regions. The high level of ionization at daytime, especially during the polar day, increases the ion drag effects and damps the AGWs in the neutral atmosphere together with their ionospheric signatures [*Tsybulya and Jakowski*, 2005]. Thus, although higher plasma density makes the observed irregularities more distinct, the ion drag significantly decreases this effect. There is also a high level of disturbance, especially on the medium scale, in the band along the geomagnetic equator. These irregularities are linked to the equatorial anomaly phenomenon. The equatorial band develops during daytime, splits into two

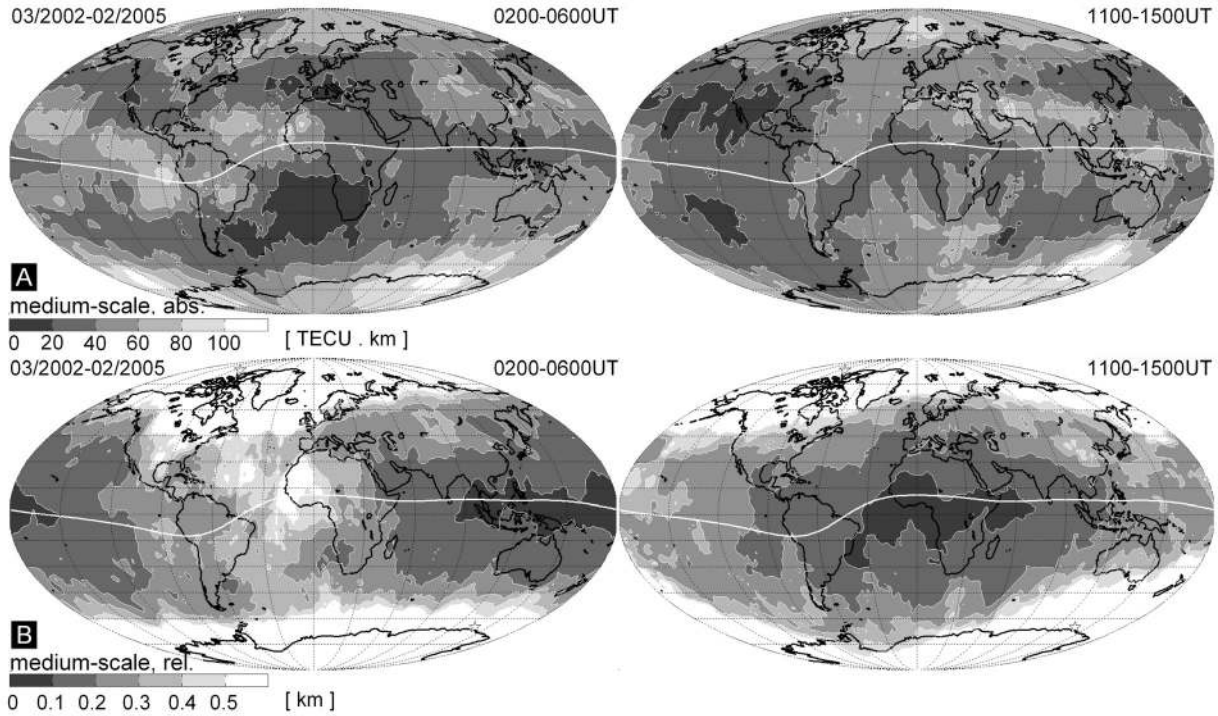

Figure 9. Medium-scale ionospheric irregularities deduced from CHAMP IRO measurements during the March 2002 to February 2005 period: (a) absolute and (b) relative intensity of ionospheric irregularities obtained (left) from 0200 to 0600 UT and (right) from 1100 to 1500 UT.

parallel subbands in the local evening hours, and gradually disappears after sunset, thus following the well-known equatorial anomaly evolution cycle. The capability to detect TIDs and related phenomena proves the IRO technique potential to enlighten the generation and propagation of ionospheric disturbances.

4. Impact of Ionospheric Disturbances on GNSS-Based Positioning

[19] In GNSS-based reference networks, the major error contributor is the differential residual error between the reference station and the rover. Since the ionospheric effects increase with the baseline length, the reference stations must be deployed in a dense enough pattern to allow for modeling the distance-dependent errors to an acceptable accuracy. A large portion of the differential ionospheric biases can be modeled and removed successfully by using observations of a network of reference stations, providing that the stations are 50–80 km apart [*Wanninger*, 2004]. Nevertheless, in the presence of small- and medium-scale ionospheric disturbances, large ionospheric residuals still remain.

[20] Integrity monitoring (for residual interpolation and ambiguity resolution) is crucial for the operational quality of the network RTK systems. The network model integrity (NMI) module [*Trimble Navigation, Ltd.*, 2005] is used to estimate the potential nonlinear residual errors in the generated data transmitted to the user and is also a very useful tool for prediction of the rover performance. To estimate the nonlinear residual error, the NMI module omits one reference station from the interpolation procedure (using adjacent stations instead) and then compares the interpolation results for that omitted station with the real measurements. It computes the interpolation error and a weighted RMS value over all satellites. The RMS values of all network stations are accumulated for each hour, and the I_{95} index [*Wanninger*, 2004] is calculated. Actually, the I_{95} index is a statistical figure, obtained from dual-frequency ambiguity-fixed carrier phase observations, providing information on the number of differential ionospheric biases. The index value is the 95% margin of all $(\Delta I_{\mathrm{Lat}}^2 + \Delta I_{\mathrm{Lon}}^2)^{1/2}$ quantities accumulated in a predefined time period (normally, 1 hour), where ΔI_{Lat} and ΔI_{Lon} are the differential ionospheric biases in south-north and west-east directions, respectively. The highest value for the respective hour is the

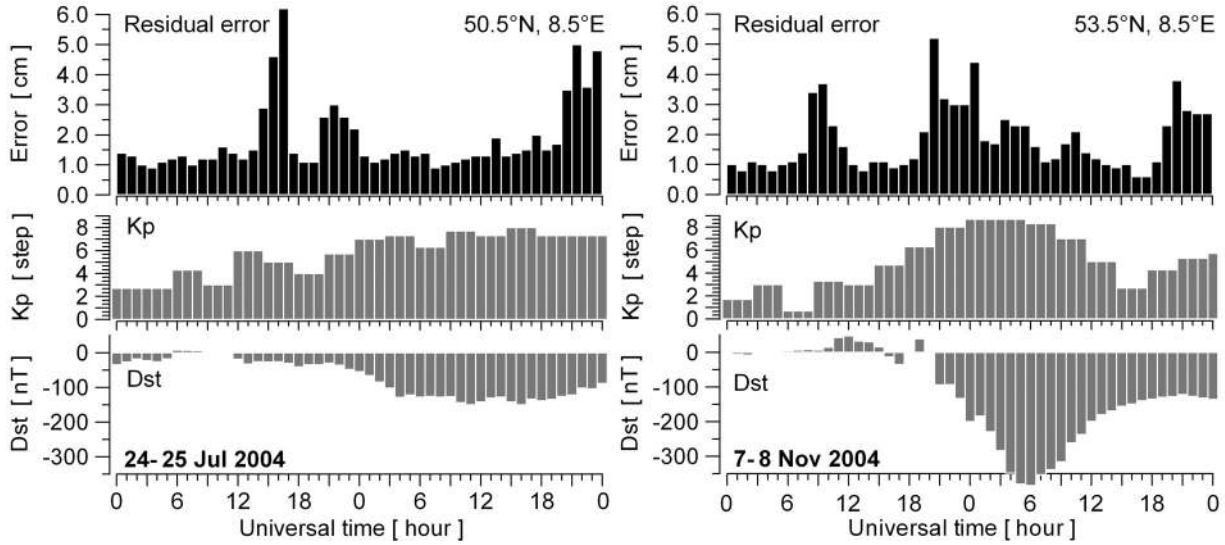

Figure 10. Network integrity monitoring during the storm periods (left) 24–25 July 2004 and (right) 7–8 November 2004. The abscissa displays the universal time, while the ordinate shows the estimated residual error.

required error estimate used by the NMI module. The experience teaches that it is hardly possible to obtain accurate positioning if the error is larger than about 8 cm [*Chen et al.*, 2003]. Nevertheless, even if the error is smaller, it may still indicate a possibility for longer than usual times to fix the ambiguities. Exemplary error estimates, obtained from operational NMI modules in Germany, are plotted for the 24 and 25 July 2004 and the 7 and 8 November 2004 storm periods (Figure 10). The influence of the ionospheric disturbances, leading to twofold to threefold increases in error (compared with the background level), is clearly visible not only during the main phases but also during the recovery phases of the storms.

5. Operational Ionosphere/Space Weather Service for GNSS Applications

[21] Motivated by the problems currently experienced by GNSS users, DLR established an operational space weather monitoring service aimed at improving GNSS positioning applications [*Jakowski et al.*, 2005]. Real-time data products are generated, such as maps of the TEC value, TEC spatial gradients, TEC rate of change (TEC_{roc}), cycle slip number, space weather alerts, etc. The products, on the basis of information about the actual and predicted state of the ionosphere-plasmasphere system, deliver only the information that reference network operators need for providing more reliable, higher-precision positioning services and for reducing the operational and other business costs. How an operational space weather monitoring service can help is demonstrated next. By generating real-time high-resolution TEC maps (Figure 11), the increased ionization in the north and its consecutive propagation in the southward/westward direction becomes obvious. As the front of the detected high-ionization (disturbance) moves through Europe, it leads to increased residual error and therefore reduced reference network integrity (cf. Figure 10). What is important to mention here is that reliable early indications of oncoming adverse storm conditions are possible to obtain only if high-resolution (spatial and temporal) mapping is available. Moreover, high resolution is crucial, particularly if small-scale phenomena are targeted. The resolution achieved by the described service so far is 1° in space, 5 min in time (update rate), and latency of less than 1 min. It is evident from the examples that the use of TEC maps only is not sufficient, particularly when addressing the ionospheric effects on network integrity; TEC gradient and TEC rate of change mapping are required as well.

6. Indexing the Local Ionospheric Response to Geomagnetic Activity

[22] The next challenge is to reliably forecast the effects caused by ionospheric disturbances. Our efforts in this direction, apart from developing an ionosphere/space weather monitoring service, include the development of a new index, which, in addition to capturing the local ionospheric response, can also enable the prediction of the ionospheric effects on GNSS-based applications.

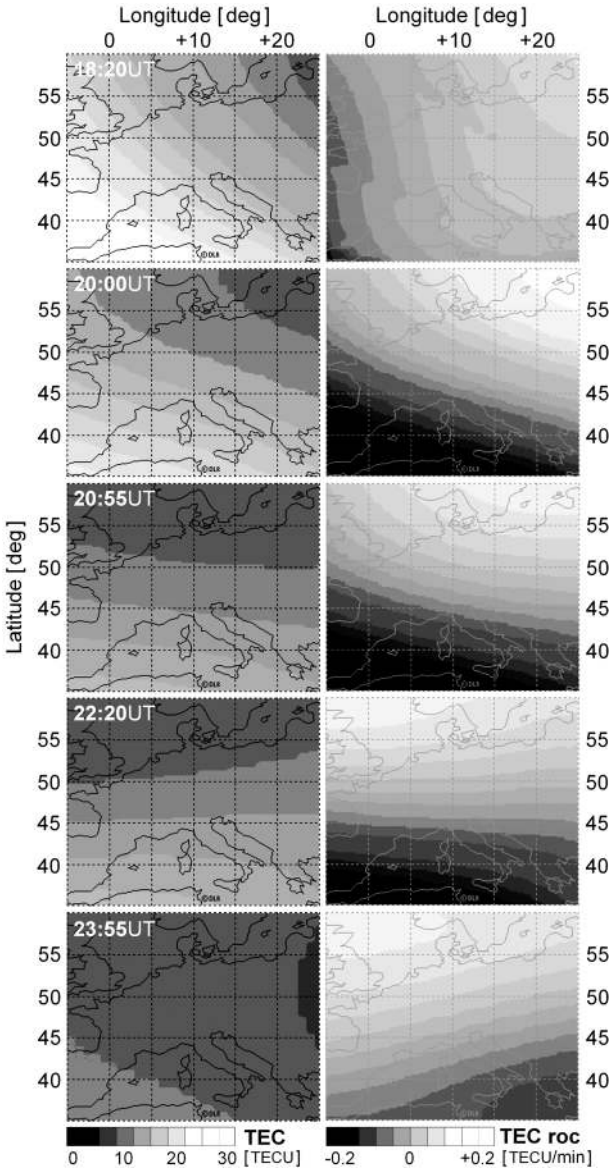

Figure 11. Operational monitoring of (left) TEC value and (right) rate of change on 7 November 2004.

An obvious problem is that the occurrence and behavior of ionospheric perturbations do not fully correlate with the behavior of the planetary geomagnetic indices that are currently available. Because of their complex interaction with the thermosphere and magnetosphere, the ionospheric perturbations cannot be described sufficiently well by using geomagnetic activity indices only. To simplify the quantitative description of ionospheric perturbation processes, we suggest the systematic introduction of ionospheric perturbation indices which describe essential features of the perturbations. Focusing on GNSS applications, a key ionospheric parameter is the total vertical ionization represented by the TEC. Being a robust integral characteristic of the ionosphere-plasmasphere system, the TEC has been successfully used in various investigations of the ionosphere and plasmasphere behavior under both quiet and disturbed conditions. TEC can effectively be monitored over large areas such as Europe, or even on a global scale. Thus, because of the importance of TEC for GNSS applications and because of the capability of using dual-frequency GNSS signals for deriving TEC maps, this parameter (and/or its derivatives) is an outstanding candidate for defining ionospheric perturbation indices. TEC-based indices may be used as input parameters in reliable forecast models and can directly be utilized to improve communications, navigation, and geodetic surveying practices. Here we only demonstrate how a prototype index based on the latitudinal gradients can be used (Figure 12). The index is obtained by averaging the TEC latitudinal gradients over a nine-point computational molecule centered at 60°N, 15°E. As seen from Figure 12, the index peaks more than an hour earlier than the maximum of the residual error's deviation from the median for a reference network located at lower latitudes, 47°N. As mentioned before, the standard geomagnetic indices (*Kp* and *Dst*) are usually not very helpful even if provided in real time.

[23] The new perturbation index [*Jakowski et al.*, 2006], provisionally named the Regional Ionosphere Disturbances Index (RIDX), has several formulations in order to better address the nature of perturbation phenomena. In the first formulation, the ionospheric perturbation parameter is defined as the standard deviation of the measurements from empirical TEC model values, that is,

$$RIDX_a^{\mathrm{mod}} = \sqrt{\left(\frac{1}{N_{\mathrm{obs}}-1}\right)\sum_{n=1}^{N\mathrm{obs}}\left(TEC_n - TEC_n^{\mathrm{mod}}\right)^2}, \tag{4}$$

where TEC_n is the vertical TEC deduced from the nth measurement, TEC^{mod} is the corresponding TEC model value, and N_{obs} is the number of simultaneous measurements. It is also possible to define the perturbation index via the TEC deviation from other nonperturbed reference values (e.g., monthly medians):

$$RIDX_r^{\mathrm{med}} = \sqrt{\left(\frac{1}{N_{\mathrm{grp}}-1}\right)\sum_{k=1}^{N\mathrm{grp}}\left[\left(TEC_k - TEC_k^{\mathrm{med}}\right)/TEC_k^{\mathrm{med}}\right]^2}, \tag{5}$$

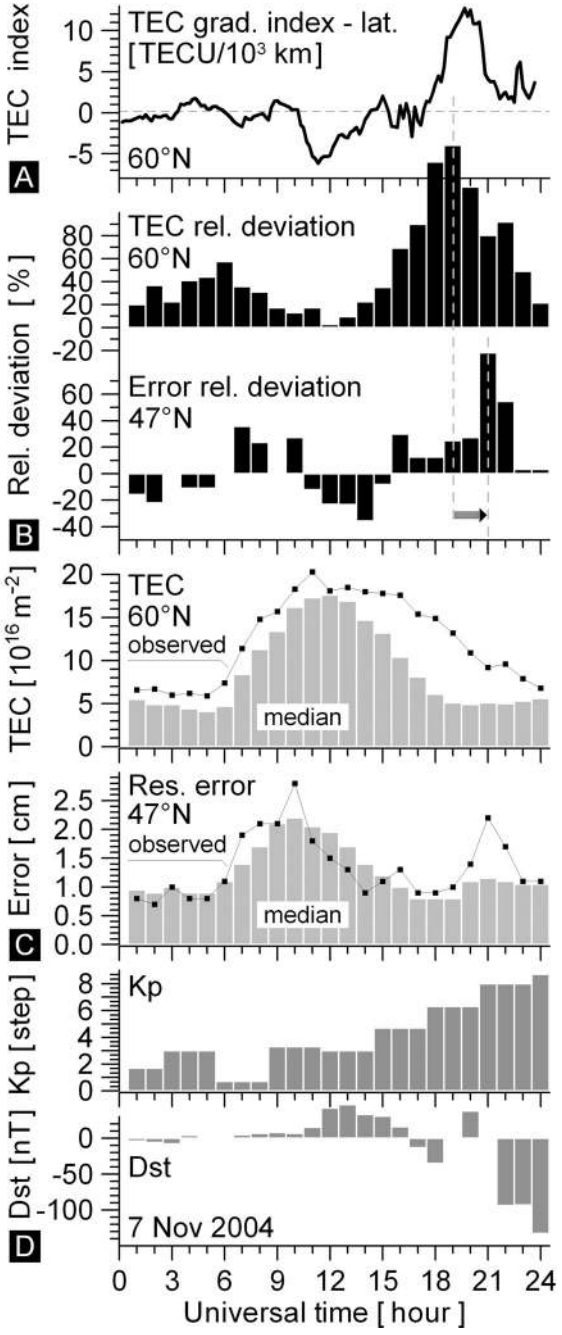

Figure 12. Indexing the local ionospheric response to ionospheric activity. (a) Latitudinal gradient index obtained from averaged TEC latitude gradient measurements at 60°N, 15°E (nine-point, 5 × 10 degree sized computational molecule used; latitude range 57.5°N–62.5°N, longitude range 10.0°E–20.0°E). (b) Relative deviations of the TEC and residual errors from the corresponding medians. (c) TEC and residual error measurements. (d) *Kp* and *Dst* indices.

where TEC_k is the vertical TEC derived for a grid point $k = (i,j)$, TEC_k^{med} is the corresponding TEC monthly median, and N_{grp} is the number of grid points in the computational molecule (or the regional map).

7. Conclusion

[24] Results from studying the generation and propagation of ionospheric disturbances by utilizing the capabilities of several modern-day techniques for routine measurements were presented. On the one hand, it was shown that the ionospheric disturbances adversely affect the performance of GNSS reference networks. On the other hand, the growing number and densification of GNSS reference networks together with the increased availability of space-based GNSS measurements onboard LEO satellites provide opportunities for more comprehensive monitoring of the ionosphere-plasmasphere system. Since the space weather–induced gradients in the electron density distribution may seriously degrade the performance of communication/navigation systems, a GNSS-based TEC monitoring service has potential forecast capability, which is a prerequisite for successful mitigation of ionospheric effects.

[25] **Acknowledgments.** This research has been funded by the German state government of Mecklenburg-Vorpommern under grant V230-630-08-TIFA-334. Space Weather Impact on Precise Positioning Applications (SWIPPA) is a project jointly supported by the German Aerospace Center and the European Space Agency (ESA) under contract ESTEC 16952/02/NL/LvH. The cooperation of the German Federal Agency for Cartography and Geodesy (BKG), E.ON Ruhrgas AG, Allsat network and services GmbH, German Research Center for Geosciences (GFZ) Potsdam, Geomagnetic Observatory Niemegk, Institute of Atmospheric Physics (IAP) Kuehlungsborn, International GPS Service (IGS), NOAA Space Environment Center (SEC), World Data Center for Geomagnetism (WDC-2) Kyoto, and Geophysical Observatory Tromsoe is gratefully acknowledged.

References

Araujo-Pradere, E. A., and T. J. Fuller-Rowell (2002), STORM: An empirical storm-time ionospheric correction model: 2. Validation, *Radio Sci.*, *37*(5), 1071, doi:10.1029/2002RS002620.

Araujo-Pradere, E. A., T. J. Fuller-Rowell, and D. Bilitza (2004), Time Empirical Ionospheric Correction Model (STORM) response in IRI2000 and challenges for empirical modeling in the future, *Radio Sci.*, *39*, RS1S24, doi:10.1029/2002RS002805.

Beutler, G., M. Rothacher, S. Schaer, T. A. Springer, J. Kouba, and R. E. Neilan (1999), The International GPS Service (IGS): An interdisciplinary service in support of Earth sciences, *Adv. Space Res.*, *23*(4), 631–635.

Blewitt, G. (1990), An automatic editing algorithm for GPS data, *Geophys. Res. Lett.*, *17*(3), 199–202.

Chen, X., H. Landau, and U. Vollath (2003), New tools for network RTK integrity monitoring, paper presented at ION GPS/GNSS 2003, Inst. of Navig., Portland, Oreg.

Foerster, M., and N. Jakowski (2000), Geomagnetic storm effects on the topside ionosphere and plasmasphere: A compact tutorial and new results, *Surv. Geophys.*, *21*(1), 47–87.

Goodman, J. M. (2005), Operational communication systems and relationships to the ionosphere and space weather, *Adv. Space Res.*, *36*(12), 2241–2252.

Heise, S., N. Jakowski, A. Wehrenpfennig, C. Reigber, and H. Lühr (2002), Sounding of the topside ionosphere/plasmasphere based on GPS measurements from CHAMP: Initial results, *Geophys. Res. Lett.*, *29*(14), 1699, doi:10.1029/2002GL014738.

Jakowski, N. (1981), A method for analyzing ionospheric perturbations by combining ionospheric total electron content with f_oF_2 data, *Phys. Solariterr.*, *15*, 130–136.

Jakowski, N. (1996), TEC monitoring by using satellite positioning systems, in *Modern Ionospheric Science*, edited by H. Kohl, R. Ruester, and K. Schlegel, pp. 371–390, Eur. Geophys. Soc., Katlenburg-Lindau, Germany.

Jakowski, N., and L. Lois (1984), Investigations of ionospheric storms by combining ionospheric total electron content with f_oF_2, *Gerlands Beitr. Geophys.*, *93*, 1–11.

Jakowski, N., A. Jungstand, K. Schlegel, H. Kohl, and K. Rinnert (1992), The ionospheric response to perturbation electric fields during the onset phase of geomagnetic storms, *Can. J. Phys.*, *70*(7), 575–581.

Jakowski, N., E. Sardon, and S. Schlueter (1998), GPS-based TEC observations in comparison with IRI95 and the European TEC model NTCM2, *Adv. Space Res.*, *22*(6), 803–806.

Jakowski, N., A. Wehrenpfennig, S. Heise, C. Reigber, H. Lühr, L. Grunwaldt, and T. K. Meehan (2002a), GPS radio occultation measurements of the ionosphere from CHAMP: Early results, *Geophys. Res. Lett.*, *29*(10), 1457, doi:10.1029/2001GL014364.

Jakowski, N., S. Heise, A. Wehrenpfennig, S. Schlueter, and R. Reimer (2002b), GPS/GLONASS based TEC measurements as a contributor for space weather forecast, *J. Atmos. Sol. Terr. Phys.*, *64*(5–6), 729–735.

Jakowski, N., S. M. Stankov, and D. Klaehn (2005), Operational space weather service for GNSS precise positioning, *Ann. Geophys.*, *23*(9), 3071–3079.

Jakowski, N., S. M. Stankov, S. Schlueter, and D. Klaehn (2006), On developing a new ionospheric perturbation index for space weather operations, *Adv. Space Res.*, in press.

Jodogne, J. C., and S. M. Stankov (2002), Ionosphere-plasmasphere response to geomagnetic storms studied with the RMI-Dourbes comprehensive database, *Ann. Geophys.*, *45*(5), 629–647.

Muhtarov, P., and I. Kutiev (1999), Autocorrelation method for temporal interpolation and short-term prediction of ionospheric data, *Radio Sci.*, *34*(2), 459–464.

Press, W. H., B. P. Flannery, S. A. Teukolsky, and W. T. Vetterling (1992), *Numerical Recipes in C*, Cambridge Univ. Press, New York.

Proelss, G. W. (1995), Ionospheric *F*-layer storms, in *Handbook of Atmospheric Electrodynamics*, vol. 2, edited by H. Volland, pp. 195–248, CRC Press, Boca Raton, Fla.

Rawer, K. (1993), *Wave Propagation in the Ionosphere*, 486 pp., Springer, New York.

Stankov, S. M. (1996), A steady-state *F*-region model and its use for satellite data analysis, *Ann. Geof.*, *39*(5), 905–924.

Stankov, S. M., and N. Jakowski (2006), Topside ionospheric scale height analysis and modelling based on radio occultation measurements, *J. Atmos. Sol. Terr. Phys.*, *68*(2), 134–162.

Stankov, S. M., N. Jakowski, S. Heise, P. Muhtarov, I. Kutiev, and R. Warnant (2003a), A new method for reconstruction of the vertical electron density distribution in the upper ionosphere and plasmasphere, *J. Geophys. Res.*, *108*(A5), 1164, doi:10.1029/2002JA009570.

Stankov, S. M., R. Warnant, and J. C. Jodogne (2003b), Real-time reconstruction of the vertical electron density distribution from GPS TEC measurements, *Acta Geod. Geophys. Hung.*, *38*(4), 377–388.

Stankov, S. M., I. S. Kutiev, N. Jakowski, and A. Wehrenpfennig (2004), GPS TEC forecasting based on auto-correlation analysis, *Acta Geod. Geophys. Hung.*, *39*(1), 1–14.

Stankov, S. M., N. Jakowski, and S. Heise (2005), Reconstruction of ion and electron density profiles from space-based measurements of the upper electron content, *Planet. Space Sci.*, *53*(9), 945–957.

Trimble Navigation, Ltd. (2005), GPSNet™ user guide, version 2.40, revision A, part 48596-24-ENG, 512 pp., Sunnyvale, Calif.

Tsunoda, R. T. (1988), High-latitude *F* region irregularities: A review and synthesis, *Rev. Geophys.*, *26*, 719–760.

Tsybulya, K., and N. Jakowski (2005), Medium- and small-scale ionospheric irregularities detected by GPS radio occultation method, *Geophys. Res. Lett.*, *32*, L09103, doi:10.1029/2005GL022420.

Wanninger, L. (2004), Ionospheric disturbance indices for RTK and network RTK positioning, paper presented at ION GNSS 2004, Inst. of Navig., Long Beach, Calif.

N. Jakowski, S. M. Stankov, K. Tsybulya, and V. Wilken, German Aerospace Center, Institute of Communications and Navigation, Kalkhorstweg 53, D-17235 Neustrelitz, Germany. (stanimir.stankov@dlr.de)